Pergamon

Int. J. Solids Structures Vol. 31, No. 15, pp. 2015–2033, 1994

0020-7683/94 $7.00 + .00

0020-7683(94)E0009-K

MECHANICS OF SPLITTING IN ORTHOTROPIC MATERIALS

YINGQING LAWRENCE CUI
Division of Applied Sciences, Harvard University, Cambridge, MA 02138, U.S.A.

(*Received* 12 *June* 1993; *in revised form* 14 *January* 1994)

Abstract—A theoretical study is made of splitting around the boundaries of elliptical holes in an orthotropic material. The splitting is modeled as a crack with both Mode I opening and Mode II sliding. The sliding resistance on the closed portion of the splitting crack is assumed to obey a Coulomb friction law. The stress intensity factors and the critical external load for splitting propagation are calculated as functions of splitting length. The dependence of stress intensity factors and the critical external load upon the length of splitting, the root radii of the hole, elastic orthotropy, frictional coefficient and the critical energy release rate is described in terms of a universal set of nondimensional parameters. It is found that splitting is unstable in the absence of frictional resistance and stable when sufficient frictional resistance is present. Elastic orthotropy, through its interaction with frictional resistance, tends to reduce the effects of frictional sliding resistance.

The stress redistribution due to splitting is also studied. It is found that the splitting is very effective in relieving the high stress concentration ahead of the tips of cracks or at the boundaries of holes. Unlike the growth of splitting itself, the stress redistribution effect is insensitive to frictional resistance. The calculated results suggest that regardless of the root radii of a flaw, a splitting crack of the length of the original flaw reduces the stress concentration factor to less than 2.

INTRODUCTION

Notches and holes are commonly required in the design of fiber composite panels. These stress concentrators are often the source of various damages in engineering structures. The stress concentration around holes is considered to be critical in the performance of engineering structural materials. For woods, aligned fibrous composites and laminated composites, splitting has been observed and recognized as an important damage phenomenon in the presence of holes and notches when the material is subjected to either tensile or compressive load (Evans, 1991; Soutis *et al.*, 1991). The typical geometry of splitting is shown in Fig. 1. Due to inhomogeneity in toughness, splitting cracks, initiating in the

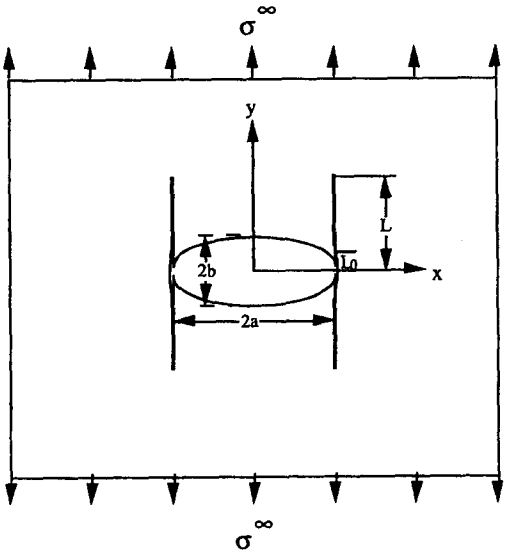

Fig. 1. Problem statement.

vicinity of a discontinuity in the forms of notches, holes and micro-flaws, are seen to propagate along geometrically particular paths such as the fiber direction of woods and aligned fibrous composites, and the interface of layered materials and laminated composites. Matrix splitting relieves the high stress concentration around hole boundaries and thus enhances both the tensile and the compressive strength of materials. The resulting stress redistribution by splitting may render the composite notch insensitive.

It is well known that debonding along a weak fiber–matrix interface is essential for a composite, be it notched or unnotched, to achieve high strength and toughness in fiber direction (Budiansky *et al.*, 1986; Budiansky and Cui, 1994). In layered systems, interface debonding is found to be very efficient in defeating cracks in individual layers and reducing the likelihood that the crack will propagate into the next layer, and it is also found that debonding can significantly promote tunnel cracking when certain conditions are met (Chan *et al.*, 1992, personal communication). Experimental study on the compression fatigue behavior of carbon fiber–epoxy laminates containing an open hole has revealed that after 10^6 cycles of compressive fatigue loading, the damage developed in the form of matrix splitting tangent to the hole *increases* the residual compressive strength of the laminate (Soutis *et al.*, 1991). Similar observations have also been made for carbon–epoxy laminates under tensile fatigue loading (Whitcomb, 1981).

Important as it is, both theoretically and practically, little work has been done to model such a phenomenon. The studies on splitting are so far limited to the special case of sharp crack-like flaws (Dollar and Steif, 1989; Chan *et al.*, 1992, personal communication). Further understanding of this mechanism is necessary for the design of composite materials.

The present study is directed to a general orthotropic material containing a center flaw in the idealized form of an elliptic hole. A model is proposed in the present study to analyze the matrix splitting and its effects on stress redistribution around a hole. For the sake of simplicity, it is assumed that both the major semi-axis and minor semi-axis of the elliptic hole are coincident with the principal axes of the material. Upon tensile loading in the direction of the minor semi-axis, matrix cracks tangent to the hole develop at both poles of the hole, as illustrated in Fig. 1. An integral equation method, which is based on distributed dislocations interacting with a free elliptic hole, is used to solve this problem. To understand the behavior of splitting, we allow both Mode I opening and Mode II sliding along the splitting crack. The interface sliding resistance along the closed part of splitting crack is characterized by a Coulomb friction model. A physical condition governing the stress free condition at the hole tip is established. This condition is essential to obtain a stable solution for the distributed dislocations. The process of splitting initiation and propagation is described. The numerical results for stress intensity factors for the splitting crack and stress concentration at the hole boundary are presented as functions of splitting length. The dependence of these quantities upon a multitude of parameters is described in terms of a universal set of nondimensional parameters. Technical issues such as the interplay between elastic orthotropy and frictional contact are rigorously addressed and their effects upon splitting propagation and stress redistribution are also discussed.

BASIC RESULTS OF ORTHOTROPIC ELASTICITY

Consider the plane strain deformation of an orthotropic material. Following Lekhnitskii (1981), if x and y axes are coincident with the principal axes of the material, Hooke's law for the material can be written as:

$$\varepsilon_{xx} = b_{11}\sigma_{xx} + b_{12}\sigma_{yy} \tag{1}$$

$$\varepsilon_{yy} = b_{12}\sigma_{xx} + b_{22}\sigma_{yy} \tag{2}$$

$$\gamma_{xy} = b_{66}\tau_{xy}. \tag{3}$$

It has been shown by Savin (1961) that the general solutions of the above plane strain problem can be expressed in terms of two analytic functions, $\phi(z_1)$ and $\psi(z_2)$ with two complex variables given by $z_1 = x+s_1 y$ and $z_2 = x+s_2 y$. The parameters s_1 and s_2 are the two roots of the algebraic equation

$$b_{11}s^4+(2b_{12}+b_{66})s^2+b_{22} = 0 \tag{4}$$

with positive imaginary parts.

In terms of $\phi(z_1)$ and $\psi(z_2)$, the stresses and displacements are given by

$$\sigma_{xx} = 2\mathrm{Re}\,[s_1^2\phi'(z_1)+s_2^2\psi'(z_2)] \tag{5}$$

$$\sigma_{yy} = 2\mathrm{Re}\,[\phi'(z_1)+\psi'(z_2)] \tag{6}$$

$$\tau_{xy} = -2\mathrm{Re}\,[s_1\phi'(z_1)+s_2\psi'(z_2)] \tag{7}$$

$$u_x = 2\mathrm{Re}\,[p_1\phi(z_1)+p_2\psi(z_2)] \tag{8}$$

$$u_y = 2\mathrm{Re}\,[q_1\phi(z_1)+q_2\psi(z_2)] \tag{9}$$

where Re[ ] denotes the real part of a complex quantity,

$$\phi' = \frac{\partial\phi}{\partial z_1}, \quad \psi' = \frac{\partial\psi}{\partial z_2},$$

and

$$p_\alpha = b_{11}s_\alpha^2+b_{12}, \quad q_\alpha = b_{22}/s_\alpha+b_{12}s_\alpha \quad \alpha = 1,2. \tag{10}$$

After introducing two nondimensional quantities (Suo, 1990)

$$\lambda = b_{11}/b_{22}, \quad \rho = (b_{12}+\tfrac{1}{2}b_{66})/(b_{11}b_{22})^{1/2} \tag{11}$$

one can express the parameters s_1 and s_2 as

$$s_1 = \frac{i(n+m)}{\lambda^{1/4}}, \quad s_2 = \frac{i(n-m)}{\lambda^{1/4}} \quad \text{for} \quad \rho > 1 \tag{12}$$

where

$$n = \sqrt{\frac{1+\rho}{2}}, \quad m = \sqrt{\frac{\rho-1}{2}}. \tag{13}$$

The singular crack tip fields, contained in the work of Sih *et al.* (1965), have been recast in terms of λ and ρ by Suo (1990). Some specific results that will be used in the present study are summarized as follows.

For a crack along the x direction, the crack opening displacements at a distance r behind the crack tip are related to the stress intensity factors by

$$\delta_y = 8b_{11}\lambda^{-3/4}nK_{\mathrm{I}}\sqrt{\frac{r}{2\pi}}, \quad \delta_x = 8b_{11}\lambda^{-1/4}nK_{\mathrm{II}}\sqrt{\frac{r}{2\pi}}. \tag{14}$$

The relationship between the energy release rate and the stress intensity is

$$G = b_{11}n(\lambda^{-3/4}K_{\mathrm{I}}^2 + \lambda^{-1/4}K_{\mathrm{II}}^2). \tag{15}$$

For a crack along the y direction, the crack opening displacements at a distance r behind the crack tip are related to the stress intensity factors by

$$\delta_x = 8b_{22}\lambda^{3/4}nK_{\mathrm{I}}\sqrt{\frac{r}{2\pi}}, \quad \delta_y = 8b_{22}\lambda^{1/4}nK_{\mathrm{II}}\sqrt{\frac{r}{2\pi}}. \tag{16}$$

The relationship between the energy release rate and the stress intensity is

$$G = b_{22}n(\lambda^{3/4}K_{\mathrm{I}}^2 + \lambda^{1/4}K_{\mathrm{II}}^2). \tag{17}$$

MODEL AND FORMULATION

The analysis of splitting in an orthotropic material is now taken up. The splitting phenomenon around a hole is modeled. A formulation, which is based on the distributed dislocations interacting with an open hole, is presented. Finally, a universal set of nondimensional parameters, which uniquely describe the splitting process, is given on the basis of a nondimensional analysis.

Model

An elliptical hole is adopted here to model general flaws. The splitting cracks develop tangent to the hole. The configuration of an elliptical hole with two doubly symmetric splitting cracks is shown in Fig. 1. Each splitting crack is of length $2L$. The major semi-axis of the ellipse is in the x direction and of length a. The minor semi-axis of the ellipse is in the y direction and of length b. Uniform tension σ^∞ in the y direction is applied at infinity. The orthotropic material, with its principal axes in the x and y directions, is assumed to undergo plane strain deformation. Due to both geometrical and load symmetries, only one of the four splitting crack branches needs to be considered. We henceforth pick the branch along $x = a$, $0 < y < L$. The variable normal stress distribution σ_{xx} produced by the uniform remote load σ^∞ along the branches in the absence of splitting cracks suggests that each splitting branch may contain two different portions: an open portion and a closed portion. For the branch under consideration, one portion of the branch, $x = a, 0 < y < L_0$, would be open, while the other portion of the branch, $x = a$, $L_0 < y < L$, would be closed. For sufficiently small L, it is anticipated that $L_0 = L$.

Denote the net normal and shear traction by $N(x, y)$ and $S(x, y)$; the boundary conditions for the open hole are

$$S(x, y) = 0 \quad N(x, y) = 0 \quad \text{on the hole boundary} \quad \frac{x^2}{a^2} + \frac{y^2}{b^2} = 1. \tag{18}$$

For the open portion of the splitting branch, the boundary conditions can be written as

$$N(a, y) = 0 \quad S(a, y) = 0 \quad 0 < y < L_0. \tag{19}$$

For the closed portion of the branch, each point undergoes frictional slipping. Frictional forces exerted across slipping interfaces have often been characterized either by a constant frictional stress or by a Coulomb friction model in the applied mechanics community. In this study, the Coulomb frictional model is used to represent the frictional resistance across the closed part of splitting crack faces. In mathematical form, the boundary conditions are

$$N(a,y) < 0 \quad L_0 < y < L \tag{20}$$

$$S(a,y) = \mu \operatorname{sgn}[h(y)]\, N(a,y) \quad L_0 < y < L \tag{21}$$

where

$$h(y) = \lim_{\varepsilon \to 0} [v(a-\varepsilon, y) - v(a+\varepsilon, y)]$$

denotes the relative shear displacement between the two faces of the splitting crack and μ is the coefficient of Coulomb friction.

The point $(x = a, y = 0)$ on the hole boundary is a very special point. It is interesting to examine the stress state of this point. There is a jump in the stress σ_{yy} between the left face and the right face of the splitting crack (see Fig. 1). We assume that the left face is broken at the intersection point $(x = a, y = 0)$ of the splitting crack and the hole boundary. The broken point is therefore stress free. Mathematically, such a condition is

$$\lim_{\varepsilon \to 0} \sigma_{yy}(a-\varepsilon^2, \varepsilon) = 0. \tag{22}$$

Formulation

The splitting cracks may be regarded as continuously distributed dislocations:

$$b_y(y) = \lim_{\varepsilon \to 0} \left[\frac{\partial v(a+\varepsilon, y)}{\partial y} - \frac{\partial v(a-\varepsilon, y)}{\partial y} \right] \quad -L \leqslant y \leqslant L \tag{23}$$

$$b_x(y) = \lim_{\varepsilon \to 0} \left[\frac{\partial u(a+\varepsilon, y)}{\partial y} - \frac{\partial u(a-\varepsilon, y)}{\partial y} \right] \quad -L_0 \leqslant y \leqslant L_0. \tag{24}$$

Now we proceed to find the solutions of the boundary value problem described in the model section by superposing two states of plane strain orthotropic elasticity for an infinite body with an elliptic hole, with the stress free conditions on the hole boundary automatically satisfied, produced as follows:

(i) apply the uniform remote loading $\sigma_{yy} = \sigma^{\infty}$.

(ii) subject all the splitting crack branches to the distributed dislocations $b_x(y)$ and $b_y(y)$, given by (23) and (24).

For each problem, we shall calculate the normal stress $\sigma_{xx}(a, y)$, shear stress $\sigma_{xy}(a, y)$ and the tip tensile stress $\lim_{\varepsilon \to 0} \sigma_{yy}(a+\varepsilon, 0)$. The superposition of the solutions of the two problems should satisfy the boundary conditions on the four splitting crack branches.

Problems (i) and (ii) may be readily handled by the complex-stress-potential method introduced in the previous section in conjunction with a conformal mapping technique. The mapping functions in the following form

$$z = \omega(\zeta) = \frac{a-b}{2}\zeta + \frac{a+b}{2}\frac{1}{\zeta} \tag{25}$$

$$z_\alpha = \omega_\alpha(\zeta) = \frac{a+is_\alpha b}{2}\zeta + \frac{a-is_\alpha b}{2}\frac{1}{\zeta} \quad \alpha = 1, 2 \tag{26}$$

map the areas outside ellipses in z, z_1, z_2 planes into the areas inside unit circles in ζ, ζ_1, ζ_2 planes, respectively. The stress potentials for problem (i) have been given by Savin (1961) as follows

$$\phi^{\infty}(\zeta_1) = \frac{a\sigma^{\infty}s_2}{2(s_1-s_2)}\zeta_1 \tag{27}$$

$$\psi^{\infty}(\zeta_2) = -\frac{a\sigma^{\infty}s_1}{2(s_1-s_2)}\zeta_2. \tag{28}$$

The solution of problem (ii) may be written on the basis of the fundamental plane strain solution for a single dislocation interacting with an open hole. The stress potentials for an edge dislocation with Burgers vectors b_x and b_y at a point (x_0, y_0) in an infinite orthotropic body are

$$\phi_0(z_1) = A\ln(z_1-z_{10}) \quad z_{10} = x_0+s_1y_0 \tag{29}$$

$$\psi_0(z_2) = B\ln(z_2-z_{20}) \quad z_{20} = x_0+s_2y_0 \tag{30}$$

where

$$A = -\frac{B_y}{\lambda^{1/4}(m+n)}+i\frac{B_x}{\lambda^{1/2}}, \quad B = \frac{B_y}{\lambda^{1/4}(n-m)}-i\frac{B_x}{\lambda^{1/2}} \tag{31}$$

with

$$B_y = \frac{b_y}{16\pi mnb_{22}}, \quad B_x = \frac{b_x}{16\pi mnb_{22}}. \tag{32}$$

In the presence of an open hole, the stress potentials of an edge dislocation may be constructed by writing ϕ^d and ψ^d in the form

$$\phi^d = \phi_0+\phi_h, \quad \psi^d = \psi_0+\psi_h. \tag{33}$$

The stress potentials ϕ_h and ψ_h have been derived by Cui (1994). In terms of B_x and B_y, these potentials can be cast into the form

$$\phi_h = F_{1x}(z_1, z_{10}, z_{20})B_x+F_{1y}(z_1, z_{10}, z_{20})B_y \tag{34}$$

$$\psi_h = F_{2x}(z_2, z_{10}, z_{20})B_x+F_{2y}(z_2, z_{10}, z_{20})B_y. \tag{35}$$

The F functions are listed in Appendix A. Integrating ϕ^d and ψ^d over the four splitting branches, one obtains the stress potentials for the problem (ii).

Superposing the solutions of problems (i) and (ii) and then substituting into conditions (19), (20) and (21) lead to the simultaneous integral equations:

$$-\frac{4m}{\lambda^{3/4}}\int_0^{L_0}\frac{B_x(y_0)}{y-y_0}\mathrm{d}y_0+\frac{1}{\lambda}\int_0^{L_0}k_{xx}(y,y_0)B_x(y_0)\,\mathrm{d}y_0 + \frac{1}{\lambda^{3/4}}\int_0^{L}k_{xy}(y,y_0)B_y(y_0)\,\mathrm{d}y_0+\sigma_{xx}^{\infty}(y) = \begin{cases} 0 & 0<y<L_0 \\ <0 & L_0<y<L \end{cases} \tag{36}$$

$$-\frac{4m}{\lambda^{1/4}}\int_0^{L}\frac{B_y(y_0)}{y-y_0}\mathrm{d}y_0+\frac{1}{\lambda^{1/2}}\int_0^{L}k_{yy}(y,y_0)B_y(y_0)\,\mathrm{d}y_0 + \frac{1}{\lambda^{3/4}}\int_0^{L_0}k_{yx}(y,y_0)B_x(y_0)\,\mathrm{d}y_0 = -\tau_{xy}^{\infty}(y)+\mu\sigma_{xx}^{\infty}(y) \quad 0<y<L \tag{37}$$

for dislocation distributions B_x and B_y, where $\sigma_{xx}^{\infty}(y)$ and $\tau_{xy}^{\infty}(y)$ are the stresses along the line of the splitting due to uniform remote tension. The kernel functions k_{xx}, k_{xy}, k_{yx} and k_{yy} are also listed in Appendix A.

It is important to note that when $L_0 = L$, both B_x and B_y have the classical square root singularity at the tip of the splitting crack. However, for $L_0 < L$, the smooth transition from opening to slipping demands that $B_x(L_0) = 0$ (Dundurs and Comninou, 1979), but B_y remains square root singular at $y = L$. For each given value of L, L_0 is determined in the solution process.

It is interesting to note that the stress jump at the intersection of the splitting crack and the hole boundary

$$\lim_{\varepsilon \to 0} [\sigma_{yy}(a+\varepsilon, 0) - \sigma_{yy}(a-\varepsilon^2, \varepsilon)]$$

is proportional to $b_y(0)$. This is because $b_y(0)$ equals the jump in strain

$$\lim_{\varepsilon \to 0} [\varepsilon_{yy}(a+\varepsilon, 0) - \varepsilon_{yy}(a-\varepsilon^2, \varepsilon)],$$

and the stress σ_{xx} is zero on both sides of the splitting crack at $x = a$, $y = 0$. Accordingly, one has

$$\lim_{\varepsilon \to 0} [\sigma_{yy}(a+\varepsilon, 0) - \sigma_{yy}(a-\varepsilon^2, \varepsilon)] = 16\pi mn B_y(0). \tag{38a}$$

Substitution of the stress free condition (22) into eqn (38a) yields

$$\lim_{\varepsilon \to 0} \sigma_{yy}(a+\varepsilon, 0) = 16\pi mn B_y(0). \tag{38b}$$

Similar argument has been made by Dollar and Steif (1992) in their work on splitting at the tips of a crack in the context of isotropic elasticity.

The tensile stress $\lim_{\varepsilon \to 0} \sigma_{yy}(a+\varepsilon, 0)$ is of great interest. This quantity is the residual stress concentration after splitting has taken place.

Equation (38b) provides a relation to implement the stress free condition (22). This may be done by calculating the quantity $\lim_{\varepsilon \to 0} \sigma_{yy}(a+\varepsilon, 0)$ in terms of integrals involving unknowns $B_x(y)$ and $B_y(y)$, and then enforcing (38b) to obtain an additional constraint for the dislocation densities. We have done so for non-zero values of the parameter $b/a\lambda^{1/4}$. For the case $b = 0$, the stress free condition degenerates to the condition of no singularities at the tip of the original flaw. Consequently, there is no need to implement the condition. However, eqn (38b) remains valid, which provides a consistency check on the solution. Note that numerical solutions for $B_x(y)$ and $B_y(y)$ also need to be verified to satisfy eqn (21).

Nondimensional parameters

Of direct significance to our understanding of splitting phenomena are the stress intensity factors K_{I}, K_{II} of the splitting crack and the associated residual stress concentration after splitting has taken place: $\lim_{\varepsilon \to 0} \sigma_{yy}(a+\varepsilon, 0)$. On the basis of eqn (16), one obtains the following relations between the stress intensity factors and the dislocation densities

$$K_{\mathrm{I}} = -\lambda^{-3/4} m (2\pi)^{3/2} \lim_{y \to L_0} \sqrt{L_0 - y}\, B_x(y) \tag{39}$$

$$K_{\mathrm{II}} = -\lambda^{-1/4} m (2\pi)^{3/2} \lim_{y \to L} \sqrt{L - y}\, B_y(y). \tag{40}$$

To proceed, we nondimensionalize our problem by introducing the nondimensional quantities:

$$B_x/\sigma^\infty\lambda^{1/4},\quad B_y/\sigma^\infty,\quad x/a,\quad y/a\lambda^{1/4},\quad b/a\lambda^{1/4},\quad L/a\lambda^{1/4}.$$

Then, one finds that the stress intensity factors take the form

$$\frac{K_I}{\sigma^\infty\sqrt{\pi a}} = \lambda^{-3/8} f(L/a\lambda^{1/4}, \rho, \lambda^{-1/4}\mu, b/a\lambda^{1/4}) \tag{41}$$

$$\frac{K_{II}}{\sigma^\infty\sqrt{\pi a}} = \lambda^{-1/8} g(L/a\lambda^{1/4}, \rho, \lambda^{-1/4}\mu, b/a\lambda^{1/4}) \tag{42}$$

and the associated parameter

$$\kappa^{\text{residual}} = \lim_{\varepsilon\to 0} \sigma_{yy}(a+\varepsilon, 0)/\sigma^\infty,$$

referred to as the residual stress concentration factor in the sense that it is the ratio of the stress at the hole tip after the event of splitting to the applied σ^∞, takes the nondimensional form

$$\kappa^{\text{residual}} = h(L/a\lambda^{1/4}, \rho, \lambda^{-1/4}\mu, b/a\lambda^{1/4}). \tag{43}$$

Substituting eqns (39) and (40) into (17) gives the energy release rate. The resulting expression is of the nondimensional form

$$\frac{G^s}{b_{22}(\sigma^\infty)^2\pi a} = [f^2(L/a\lambda^{1/4}, \rho, \lambda^{-1/4}\mu, b/a\lambda^{1/4}) + g^2(L/a\lambda^{1/4}, \rho, \lambda^{-1/4}\mu, b/a\lambda^{1/4})]n. \tag{44}$$

We note that the root radii R of an elliptic hole is related to the aspect ratio b/a via $R/a = (b/a)^2$. We note also that parameters $\lambda^{-1/4}\mu$ and $b/a\lambda^{1/4}$ are no longer the frictional coefficient and the aspect ratio of the hole due to the presence of elastic orthotropy. We will discuss the implications of these parameters in detail in the discussions that follow.

RESULTS AND DISCUSSIONS

We begin by a brief discussion of the initiation of matrix splitting and then present the results for both Mode I and II stress intensity factors and describe the features of splitting cracking for the orthotropic material with an elliptic hole over a wide range of values of the aspect ratio $b/a\lambda^{1/4}$. This is followed by the discussion of propagation and stability of the splitting process. Finally, we present the calculated results for the residual stress concentration factor and discuss the stress redistribution due to splitting. In each section, the results for $\rho = 1$ with no frictional resistance is presented first. The effects of orthotropy and frictional resistance are then discussed.

Initiation

The initiation of matrix splitting tangent to a hole is a very complicated problem. It is believed that shear stress is the dominant driving force in the initiation process. At the point $(x = a, y = 0)$ on the hole boundary, both shear stress τ_{xy} and transverse tensile stress σ_{xx} are zero. The prediction of the exact location of the initiation along the line of splitting is still largely an unresolved problem. We will not pursue this any further in the present study. We nevertheless assume that splitting begins at the point $(x = a, y = 0)$ on the hole boundary.

The initiation of matrix splitting from a crack tip, corresponding to $b = 0$ in the present study, is a well defined problem. A recent experimental study (Sbaizero *et al.*, 1990) on splitting crack initiation in laminated ceramic–matrix composites has shown that the critical energy release rate for splitting initiation from the tips of a precut notch is almost the same

($G_c \approx 15$–$20\ \mathrm{J \cdot m^{-2}}$, where G_c denotes the critical energy release rate for splitting initiation) for a number of specimens with different numbers of layers. This striking evidence suggests that a common mechanism is involved, and that the splitting cracking initiation process can be well characterized by a critical energy release rate. Such a critical energy release rate is an intrinsic material property. In the light of the above observations, we present the energy release rate to initiate a splitting crack at the tip of a parent crack by taking the limit $L/a\lambda^{1/4} \to 0$ and $b/a\lambda^{1/4} \to 0$ in eqn (44). For sufficiently small values of $L/a\lambda^{1/4}$, every point along the splitting branch is open. No frictional stress is transmitted across the crack faces. The driving force G^S is therefore independent of the frictional constant μ. In the limit of $L/a\lambda^{1/4} \to 0$ and $b/a\lambda^{1/4} \to 0$, the nondimensional energy release rate $G^S/b_{22}(\sigma^\infty)^2\pi a$ depends only upon the parameter ρ. The energy release rate G^S thus takes the form

$$G^S = b_{22}H(\rho)(\sigma^\infty)^2\pi a. \tag{45}$$

A plot of $H(\rho)$ is shown in Fig. 2 for $1 < \rho < 5$. For $\rho = 1$, $H(1) = 0.263$, in agreement with the result of Chan *et al.* (1992, personal communication). As ρ is increased from 1 to 5, the nondimensional energy release rate is increased by 30%.

The stress required for splitting initiation can be obtained by setting $G^S = G_c$. The resulting external load is

$$\sigma^\infty = \sqrt{\frac{G_c}{H(\rho)b_{22}\pi a}}. \tag{46}$$

Equation (46) suggests a way to estimate the intrinsic parameter of an interface. By measuring the critical loading required to initiate a splitting along the interface, one can obtain the critical interface debonding energy G_c from the following equation

$$G_c = (\sigma^\infty)^2H(\rho)b_{22}\pi a. \tag{47}$$

Stress intensity factors

A qualitative description of the features of splitting is as follows. Regardless of the values of the aspect ratio $b/a\lambda^{1/4}$, there are two distinct stages of splitting. At the first stage, the splitting crack is fully open and the crack tip at the end of the splitting is subjected to mixed mode condition. The first stage lasts until $L/a\lambda^{1/4}$ reaches a critical value $L_c/a\lambda^{1/4}$. For $L/a\lambda^{1/4} > L_c/a\lambda^{1/4}$, the splitting crack tip is closed and therefore in a state of pure Mode II. However, one portion of the splitting crack near the hole tip remains open.

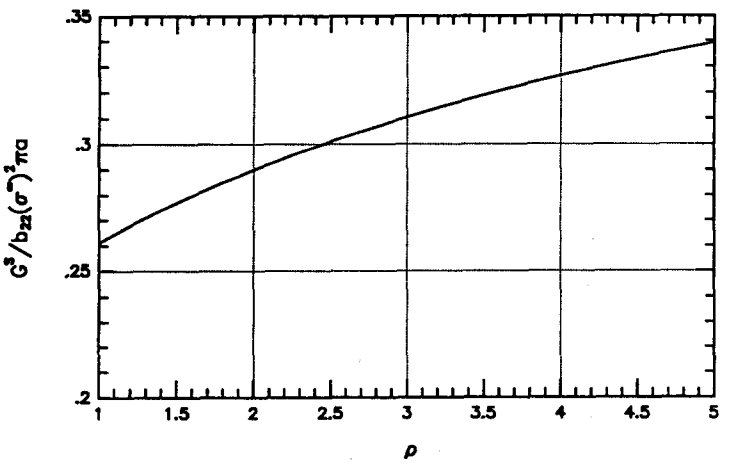

Fig. 2. Energy release rate for splitting initiation from the tip of a crack $G^S/b_{22}(\sigma^\infty)^2\pi a$ vs orthotropic parameter ρ.

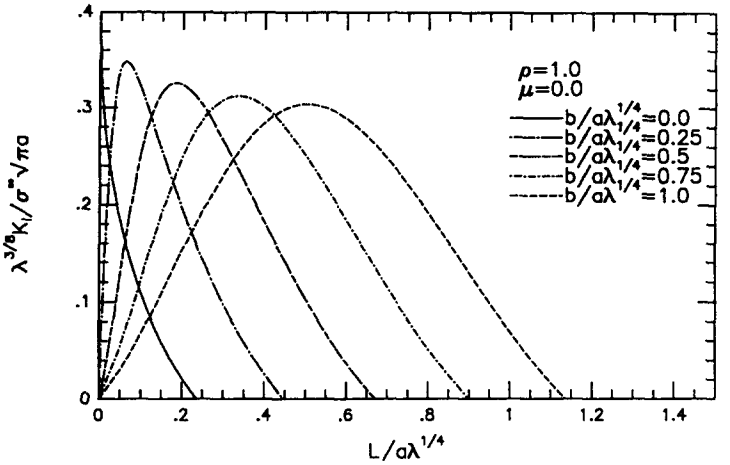

Fig. 3. Mode I stress intensity factor $\lambda^{3/8}K_I/\sigma^\infty\sqrt{\pi a}$ vs $L/a\lambda^{1/4}$, various $b/a\lambda^{1/4}$.

The stress intensity factors were calculated from eqns (39) and (40) after solving for B_x, B_y and L_0 from a system of the simultaneous integral equations (36), (37) and the constraint (38), as described in the previous section.

Consider first frictionless contact ($\mu = 0$). The nondimensional Mode I stress intensity factor $\lambda^{3/8}K_I/\sigma^\infty\sqrt{\pi a}$ is given in Fig. 3 for $\rho = 1$, and several values of aspect ratio $b/a\lambda^{1/4}$. For the limit $b/a\lambda^{1/4} = 0$, as $L/a\lambda^{1/4}$ is increased from zero to roughly 0.24, the nondimensional stress intensity factor decreases monotonically from a finite value to zero, in agreement with the results of Dollar and Steif (1989). For non-zero values of $b/a\lambda^{1/4}$, the Mode I stress intensity factor starts at zero, increases to a maximum and then drops to zero at the critical value $L_c/a\lambda^{1/4}$. This is consistent with the tensile stress distribution $\sigma_{xx}(a, y)$ produced by the remote uniform load σ^∞ along the line of the splitting branch. The critical length $L_c/a\lambda^{1/4}$ increases from about 0.24 for $b/a\lambda^{1/4} = 0$ to approximately 1.15 for $b/a\lambda^{1/4} = 1$. An inspection of Fig. 3 indicates that the length of mixed mode cracking zone L_c is always greater than the length of the minor semi-axes b, and that the mixed mode cracking zone for a circular hole is much longer than that for a crack.

The nondimensional Mode II stress intensity factor $\lambda^{1/8}K_{II}/\sigma^\infty\sqrt{\pi a}$ is presented in Fig. 4 for the same values of parameters as those in Fig. 3. The Mode II stress intensity factor first experiences an increase, then decreases and asymptotes toward a steady state value. For the limit $b/a\lambda^{1/4} = 0$, the results are in excellent agreement with those of Dollar and Steif (1989). At a given length of splitting crack, the Mode II stress intensity factor $\lambda^{1/8}K_{II}/$

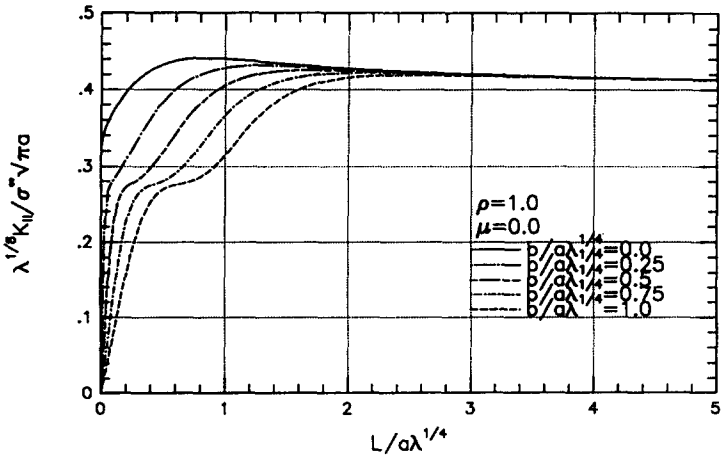

Fig. 4. Mode II stress intensity factor $\lambda^{1/8}K_{II}/\sigma^\infty\sqrt{\pi a}$ vs $L/a\lambda^{1/4}$, various $b/a\lambda^{1/4}$.

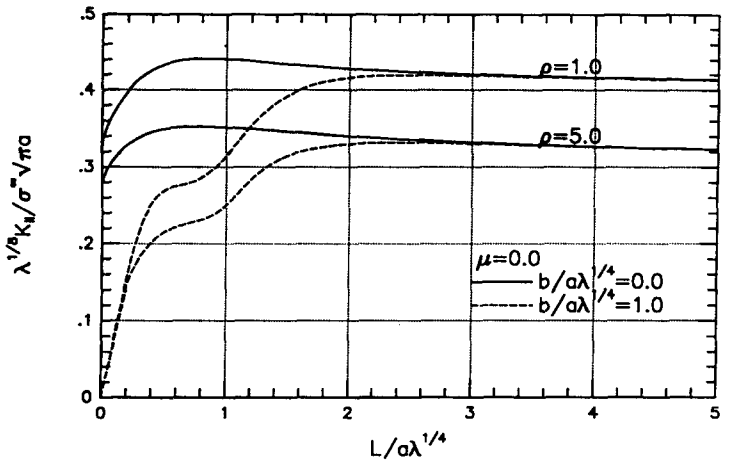

Fig. 5. Mode II stress intensity factor $\lambda^{1/8}K_{II}/\sigma^{\infty}\sqrt{\pi a}$ vs $L/a\lambda^{1/4}$, $\rho = 1, 5$ and $b/a\lambda^{1/4} = 0, 1$.

$\sigma^{\infty}\sqrt{\pi a}$ is the maximum for $b = 0$, and decreases with increasing values of the aspect ratio $b/a\lambda^{1/4}$. It is seen that for $L/a\lambda^{1/4} < 2$, the stress intensity factor $\lambda^{1/8}K_{II}/\sigma^{\infty}\sqrt{\pi a}$ is sensitive to the aspect ratio $b/a\lambda^{1/4}$. However, for $L/a\lambda^{1/4} > 3$, the aspect ratio has little influence upon the nondimensional stress intensity factor.

To examine the effects of ρ, we calculated the Mode II stress intensity factor $\lambda^{1/8}K_{II}/\sigma^{\infty}\sqrt{\pi a}$ for $\rho = 5$ (the upper limit of the parameter for a number of engineering materials), $\mu = 0$, and $b/a\lambda^{1/4} = 0$ and 1. The results are plotted in Fig. 5. Also plotted in Fig. 5 are the corresponding results for $\rho = 1$. As ρ is increased from 1 to 5, the stress intensity factor $\lambda^{1/8}K_{II}/\sigma^{\infty}\sqrt{\pi a}$ is reduced by roughly 25%. We notice that, for a given value of ρ, $\lambda^{1/8}K_{II}/\sigma^{\infty}\sqrt{\pi a}$ asymptotes toward the same steady state value regardless of the values of the aspect ratio $b/a\lambda^{1/4}$.

The Mode II stress intensity factor $\lambda^{1/8}K_{II}/\sigma^{\infty}\sqrt{\pi a}$ also depends upon the parameter $\lambda^{-1/4}\mu$. The effects of frictional resistance upon the Mode II stress intensity factor $\lambda^{1/8}K_{II}/\sigma^{\infty}\sqrt{\pi a}$ are shown in Figs 6 and 7 for $\rho = 1$, and various values of the parameter $\lambda^{-1/4}\mu$, with $b/a\lambda^{1/4} = 1$, respectively. The effects of $\lambda^{-1/4}\mu$ upon the Mode II stress intensity factor are roughly the same for $b/a\lambda^{1/4} = 0$ and $b/a\lambda^{1/4} = 1$. Frictional resistance becomes active only after splitting length $L/a\lambda^{1/4}$ reaches the critical value $L_c/a\lambda^{1/4}$. For small values of $\lambda^{-1/4}\mu$, the Mode II stress intensity factor first experiences a peak after the frictional resistance becomes operative and then decreases with increasing splitting length $L/a\lambda^{1/4}$.

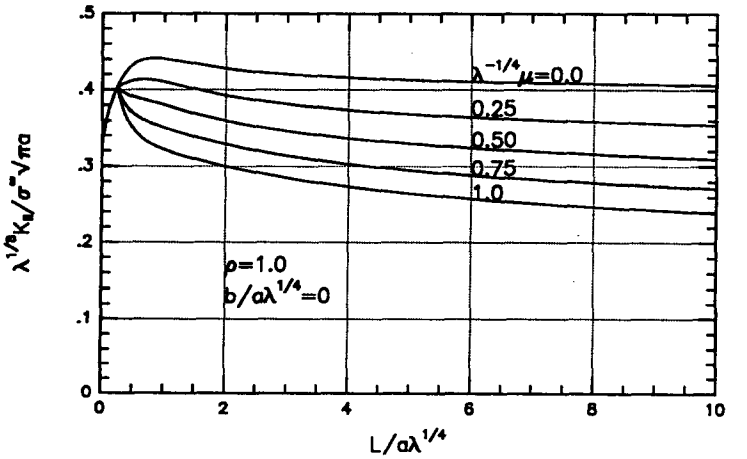

Fig. 6. Mode II stress intensity factor $\lambda^{1/8}K_{II}/\sigma^{\infty}\sqrt{\pi a}$ vs $L/a\lambda^{1/4}$, $b/a\lambda^{1/4} = 0$, various $\lambda^{-1/4}\mu$.

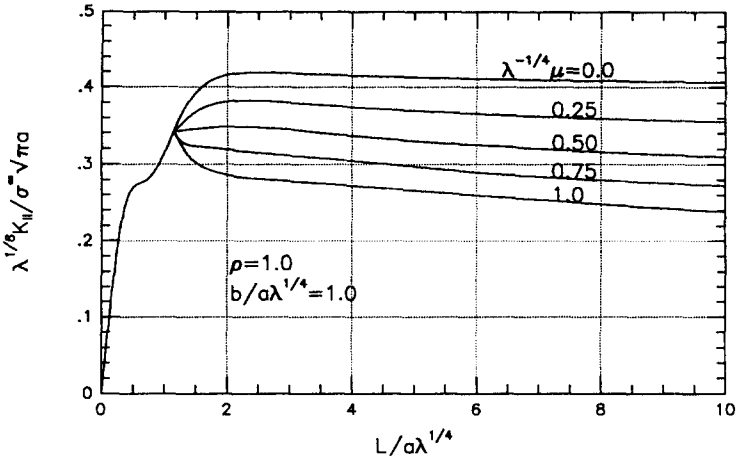

Fig. 7. Mode II stress intensity factor $\lambda^{1/8}K_{II}/\sigma^{\infty}\sqrt{\pi a}$ vs $L/a\lambda^{1/4}$, $b/a\lambda^{1/4} = 1$, various $\lambda^{-1/4}\mu$.

For large values of $\lambda^{-1/4}\mu$, the Mode II stress intensity factor decreases monotonically with increasing splitting length $L/a\lambda^{1/4}$ as soon as the frictional resistance becomes operative. For a fixed length of splitting crack, the stress intensity factor $\lambda^{1/8}K_{II}/\sigma^{\infty}\sqrt{\pi a}$ decreases with the increasing values of $\lambda^{-1/4}\mu$. The implication of the combination of the parameters $\lambda^{-1/4}$ and μ will be discussed in the next section.

Propagation

The splitting propagation under mixed mode condition is a complex problem. The experimental observations (Cao and Evans, 1989) suggest that under mixed-mode loading the critical energy release rate is not a fixed quantity but a function of the ratio of K_{II} to K_I. However, the problem of splitting propagation under pure Mode II condition is much better defined in the sense that a critical energy release rate can be unambiguously defined. Attention is therefore focused on the behavior of the splitting propagation under pure Mode II condition. Let G_{II}^c denote the critical energy release rate for the splitting to propagate under pure Mode II conditions. Imposing the condition, $G^S = G_{II}^c$, one obtains

$$\frac{\sigma^{\infty}\sqrt{b_{22}n\pi a}}{\sqrt{G_{II}^c}} = \frac{1}{g(L/a\lambda^{1/4}, \rho, \lambda^{-1/4}\mu, b/a\lambda^{1/4})}. \tag{48}$$

Consider first the results given by (48) for the case of frictionless contact. Shown in Fig. 8 are the results for $\sigma^{\infty}\sqrt{b_{22}n\pi a}/\sqrt{G_{II}^c}$ vs $L/a\lambda^{1/4}$ for $\rho = 1$, $\mu = 0$ and several values of $b/a\lambda^{1/4}$. The start of each curve corresponds to the critical value of $L_c/a\lambda^{1/4}$ at which the condition of the splitting crack tip changes from open to closed. The critical load $\sigma^{\infty}\sqrt{b_{22}n\pi a}/\sqrt{G_{II}^c}$ required to propagate the splitting is the maximum at the start of each curve. Unless unloading takes place, the splitting would propagate dynamically as soon as the maximum critical load mentioned above is reached. In this sense, Fig. 8 demonstrates that the splitting propagation is unstable in the absence of frictional resistance.

The effect of frictional resistance upon splitting propagation process is shown in Fig. 9 where the results of $\sigma^{\infty}\sqrt{b_{22}n\pi a}/\sqrt{G_{II}^c}$ vs $L/a\lambda^{1/4}$ have been plotted for $\rho = 1$, $b/a\lambda^{1/4} = 0$ and several values of the parameter $\lambda^{-1/4}\mu$. Firstly, we note that frictional resistance stabilizes the splitting propagation process. Secondly, we note that there is a strong dependence of the splitting propagation stress on the parameter $\lambda^{-1/4}\mu$, which conveniently characterizes the interaction between elastic orthotropy and frictional contact. Thirdly, the combination $\lambda^{-1/4}\mu$ suggests that elastic orthotropy tends to contract the coefficient of Coulomb friction by a factor of $\lambda^{1/4}$. This result can also be extended to the case where a constant friction stress is used to characterize the frictional resistance. For this case, the

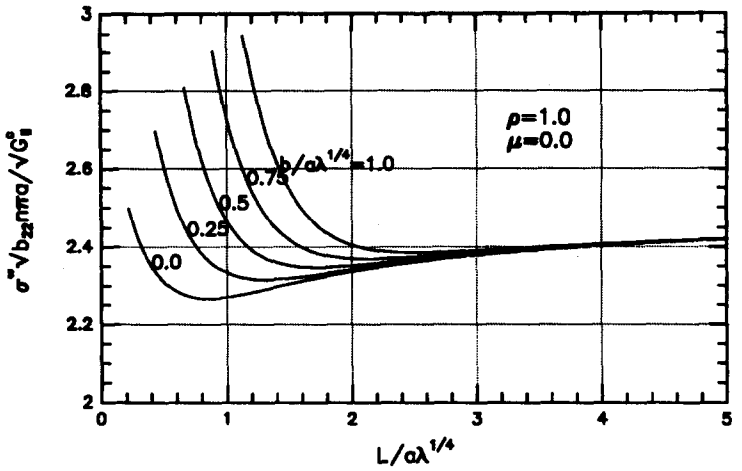

Fig. 8. Critical stress for splitting propagation under pure Mode II condition $\sigma^{\infty}\sqrt{b_{22}\pi a}/\sqrt{G_{II}^{c}}$ vs $L/a\lambda^{1/4}$ for $\mu = 0$, various $b/a\lambda^{1/4}$.

constant frictional stress is also contracted by a factor of $\lambda^{1/4}$. This is of significant technical consequence, since it has been confirmed experimentally that splitting cracking is strongly resisted by fiber cross-over or matrix ligament bridging that leads to resistance curves (de Charentenay *et al.*, 1984; Sbaizero *et al.*, 1990).

Stress concentration and stress redistribution

We shall now discuss the stress redistribution due to matrix splitting. The role of matrix splitting on reducing the stress concentration is displayed in Fig. 10, where the ratio of the stress concentration after splitting to the remote applied stress σ^{∞} (residual stress concentration factor) is plotted against the normalized splitting length $L/a\lambda^{1/4}$ for $b/a\lambda^{1/4} = 0$, 1 with $\mu = 0$. Matrix splitting is clearly very effective in reducing the stress concentration at hole boundary, even for a small amount of splitting. At $L/a\lambda^{1/4} = 3$, the high stress concentration has almost been eliminated. Observe that the residual stress concentration factor is little influenced by the values of the parameter $b/a\lambda^{1/4}$ when the splitting crack is sufficiently long. An inspection of Fig. 11 indicates that the difference in the nondimensional residual stress concentration factor $\sigma_{yy}(a^{+}, 0)/\sigma^{\infty}$ is less than 5% when the aspect ratio $b/a\lambda^{1/4}$ is changed from 0 to 1 for $L/a\lambda^{1/4} > 2$. Also plotted in Fig. 10 are

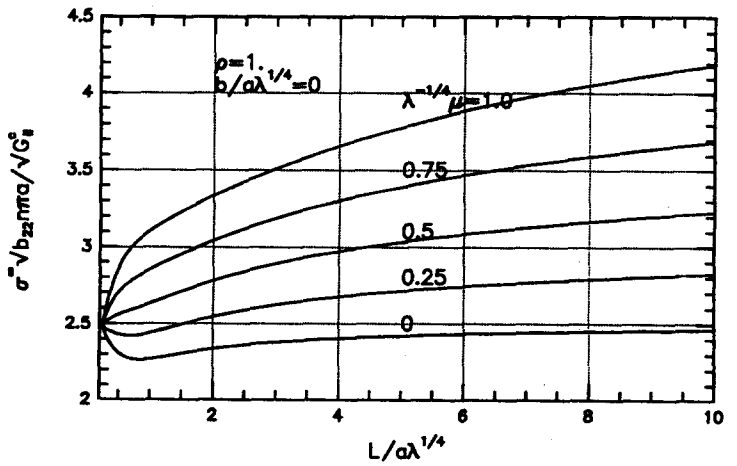

Fig. 9. Critical stress for splitting propagation under pure Mode II condition $\sigma^{\infty}\sqrt{b_{22}\pi a}/\sqrt{G_{II}^{c}}$ vs $L/a\lambda^{1/4}$ for $b/a\lambda^{1/4} = 0$, various $\lambda^{-1/4}\mu$.

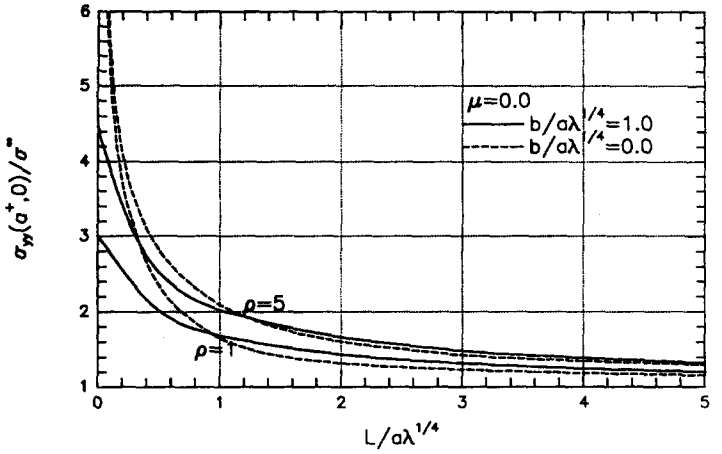

Fig. 10. Residual stress concentration factor $\sigma_{yy}(a^+,0)/\sigma^\infty$ vs $L/a\lambda^{1/4}$ for $\mu = 0$, $b/a\lambda^{1/4} = 0$, 1 and $\rho = 1$, 5.

the corresponding results for $\rho = 5$. The curves suggest that ρ doesn't have significant effect on reducing the stress concentration.

To further illustrate the effects of notch root radii, we plot the results of the ratio of residual stress concentration factor κ^{residual} to the stress concentration factor without splitting κ_0, given by

$$\kappa_0 = 1 + 2n\lambda^{1/4}a/b \tag{49}$$

which is obtained by substituting eqns (27) and (28) into (6). The results are shown in Fig. 11 for various values of the aspect ratio $b/a\lambda^{1/4}$ with $\mu = 0$. This figure makes it clear that the smaller the aspect ratio $b/a\lambda^{1/4}$, the more effective the matrix splitting is in reducing the stress concentration.

To further explore the stress redistribution effects, we now examine how the stress profile $\sigma_{yy}(x, 0)$ ahead of the hole tip may be changed from that of without splitting. Figures 12–15 show not only the decrease of stress concentration at the hole tip with the increase in the length of splitting, but also the change in the shape of the stress profile $\sigma_{yy}(x, 0)$ for $\rho = 1$, $\mu = 0$, various levels of splitting length, and several values of aspect ratio $b/a\lambda^{1/4}$. In Figs 12–15, solid curves represent the stress profiles $\sigma_{yy}(x, 0)$ corresponding to the critical values of splitting length $L_c/a\lambda^{1/4}$ when the tips of the splitting cracks change from open

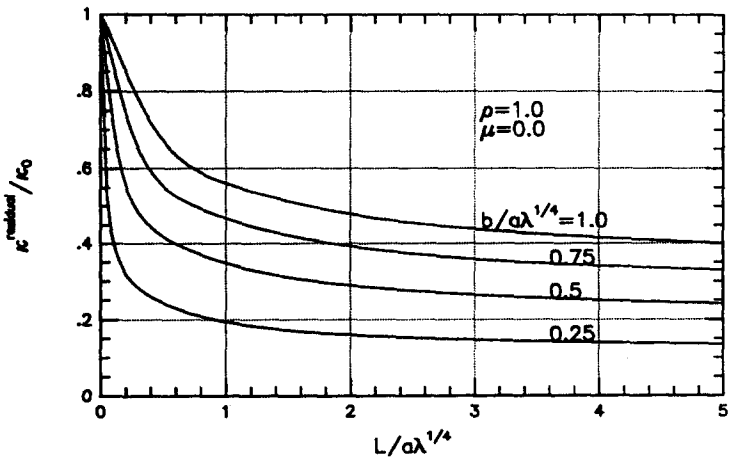

Fig. 11. The ratio of the residual stress concentration factor to that of without splitting $\kappa^{\text{residual}}/\kappa_0$ vs $L/a\lambda^{1/4}$, various $b/a\lambda^{1/4}$.

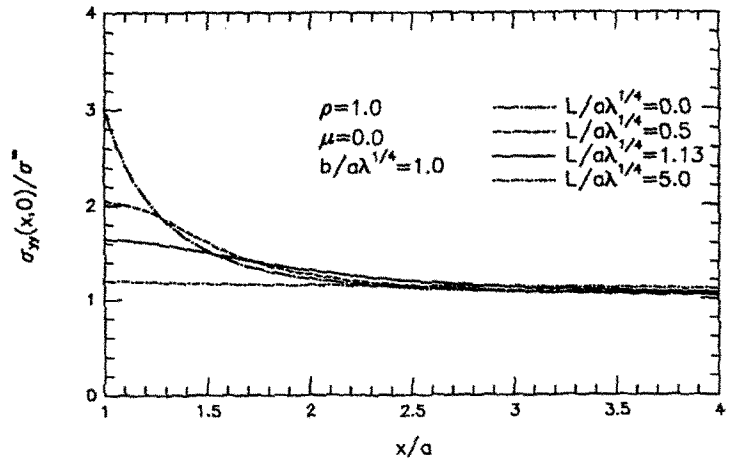

Fig. 12. Stress profiles ahead of hole tips $\sigma_{yy}(x,0)/\sigma^{\infty}$ for $b/a\lambda^{1/4} = 1$, various levels of splitting $L/a\lambda^{1/4}$.

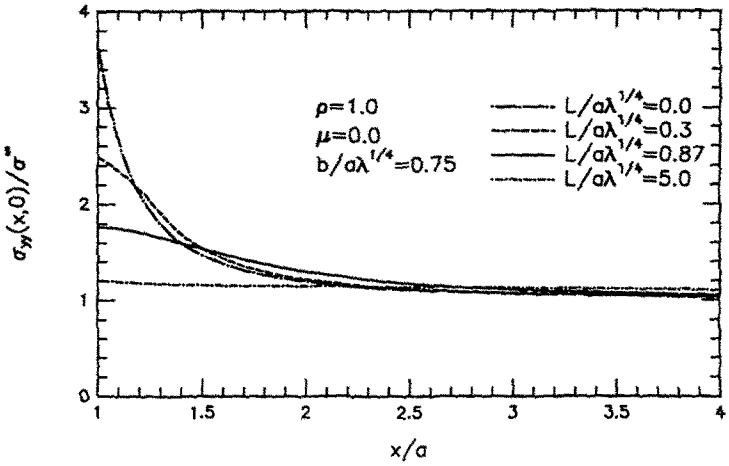

Fig. 13. Stress profiles ahead of hole tips $\sigma_{yy}(x,0)/\sigma^{\infty}$ for $b/a\lambda^{1/4} = 0.75$, various levels of splitting $L/a\lambda^{1/4}$.

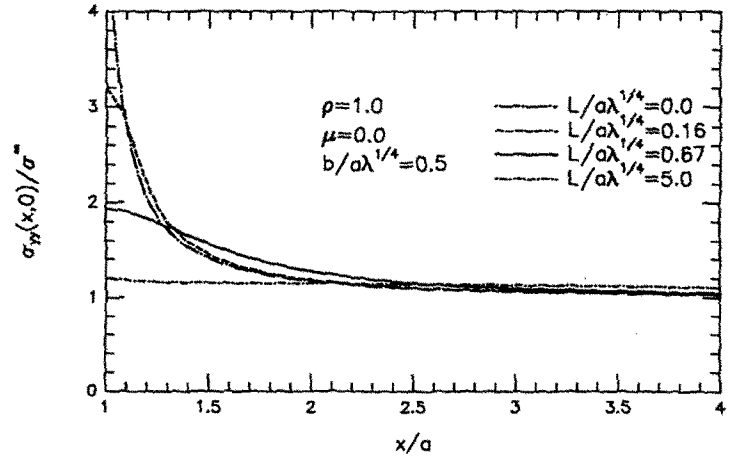

Fig. 14. Stress profiles ahead of hole tips $\sigma_{yy}(x,0)/\sigma^{\infty}$ for $b/a\lambda^{1/4} = 0.5$, various levels of splitting $L/a\lambda^{1/4}$.

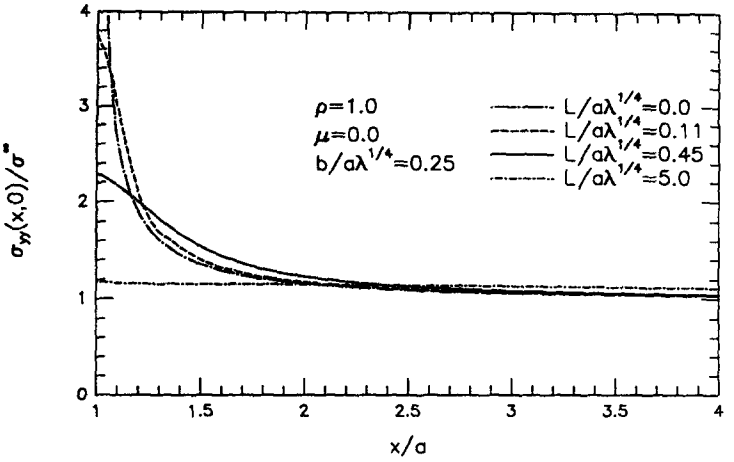

Fig. 15. Stress profiles ahead of hole tips $\sigma_{yy}(x,0)/\sigma^{\infty}$ for $b/a\lambda^{1/4} = 0.25$, various levels of splitting $L/a\lambda^{1/4}$.

(under mixed condition) to closed (under pure Mode II condition). These figures clearly indicate that the stress concentration has been significantly reduced even before the tip of the splitting becomes closed.

To study the effects of friction upon reducing the stress concentration, we plot the results of residual stress concentration factor for various values of $\lambda^{-1/4}\mu$ for $b/a\lambda^{1/4} = 0$. The results are given in Fig. 16. It is seen that the reduction in stress concentration factor has been reduced to some extent in the presence of frictional resistance. However the frictional resistance becomes operative only after the tip of the splitting crack becomes closed. In addition, the stress concentration has already been reduced drastically before the frictional resistance becomes operative. Consequently, we conclude that frictional resistance doesn't have a significant effect on stress redistribution.

It is interesting to note that even for a very small splitting crack, the stress concentration factor is reduced significantly. This may partially explain why fiber breakage ahead of notches and holes is rarely observed in experiments.

CONCLUDING REMARKS

The present study has provided the complete solutions to the matrix splitting around the tips of cracks or holes in orthotropic materials, when subjected to uniform remote

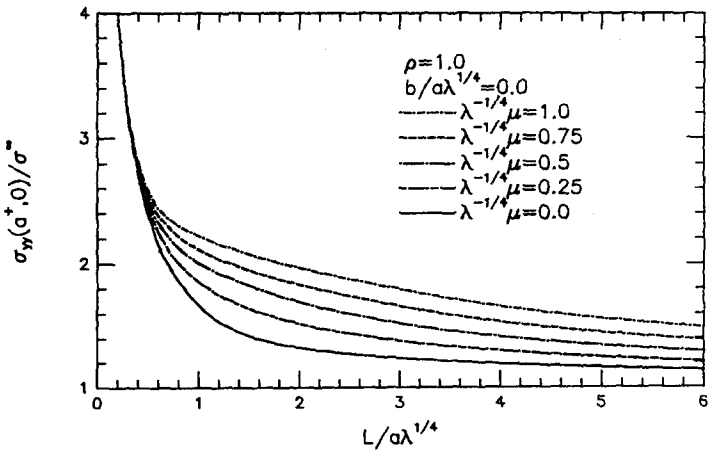

Fig. 16. Residual stress concentration factor $\sigma_{yy}(a^{+},0)/\sigma^{\infty}$ vs $L/a\lambda^{1/4}$ for $b/a\lambda^{1/4} = 0$, various $\lambda^{-1/4}\mu$.

tensile loading. The basic analysis and quantitative results presented in this paper, encompassing effects of elastic orthotropy, splitting crack initiation and growth, frictional resistance and stress redistribution, provided a broad basis for the understanding of the splitting phenomenon. In particular, it is found that the interaction between elastic anisotropy and frictional sliding tends to reduce the effects of frictional resistance and such a reduction can be conveniently measured by an interaction parameter $\lambda^{-1/4}\mu$. Splitting is found to be very effective in reducing the notch sensitivity of engineering materials and in preventing fibers ahead of the hole tips from fracture. Although it plays a significant role in stabilizing splitting matrix crack growth, frictional resistance has little influence on the stress redistribution. The numerical results suggest that the higher the stress concentration, the more effective the stress redistribution due to the splitting. We found that the stress concentration factor has been reduced to less than 2 for a splitting crack of the length of the original flaw over a wide range of the values of the aspect ratio $b/a\lambda^{1/4}$.

Acknowledgment—The author is very grateful to Professors B. Budiansky and A. G. Evans for their encouragement and their comments on this work. Discussions with Professor J. W. Hutchinson have been very helpful. This work was partially supported by the DARPA University Research Initiative (Subagreement P.O. #VB38639-0 with the University of California, Santa Barbara, ONR Prime Contract N00014-86-K-0753 and Subagreement P.O. #KK3007 with the University of California, Santa Barbara, ONR Prime Contract N00014-92-J-1808), the Office of Naval Research (Contract N00014-90-J-1377), and by the Division of Applied Sciences, Harvard University.

REFERENCES

Budiansky, B. and Cui, Y. L. (1994). On the tensile strength of a fiber-reinforced ceramic composite containing a crack-like flaw. *J. Mech. Phys. Solids* **42**, 1–19.

Budiansky, B., Hutchinson, J. W. and Evans, A. G. (1986). Matrix fracture in fiber-reinforced ceramics. *J. Mech. Phys. Solids* **34**, 167–189.

Cao, H. C. and Evans, A. G. (1989). An experimental study of the fracture resistance of bimaterial interface. *Mech. Mater.* **7**, 295–305.

Cui, Y. L. (1994). An elliptical inclusion in an anisotropic plane. To be published.

de Charentenay, F. X., Harry, J. M., Prel, Y. J. and Benzeggagh, M. L. (1984). Characterizing the effect of delamination defect by mode I delamination test. *Effect of Defects in Composite Materials*. ASTM STP 836, pp. 84–103. Philadelphia, PA.

Dollar, A. and Steif, P. S. (1989). The branched problem revisited. *ASME J. Appl. Mech.* **56**, 584–586.

Dollar, A. and Steif, P. S. (1992). Interface blunting of matrix cracks in fiber-reinforced ceramics. *ASME J. Appl. Mech.* **59**, 797–803.

Dundurs, J. and Comninou, M. (1979). Some consequences of the inequality conditions in contact and crack problems. *J. Elast.* **9**, 71–82.

Evans, A. G. (1991). The mechanical properties of reinforced ceramic, metal and inter metallic matrix composites. *Mater. Sci. Engng* **A143**, 63–76.

Lekhnitskii, S. G. (1981). *Theory of Elasticity of an Anisotropic Body*. Mir Publishers, Moscow.

Savin, G. N. (1961). *Stress Concentration Around Holes*. Pergamon, Oxford.

Sbaizero, O., Charalambides, P. G. and Evans, A. G. (1990). Delamination cracking in laminated ceramic matrix composites. *J. Am. Ceramic Soc.* **73**, 1936–1940.

Sih, G. C., Paris, P. C. and Irwin, G. R. (1965). On cracks in rectilinearly anisotropic bodies. *Int. J. Fracture Mech.* **1**, 189–203.

Suo, Z. (1990). Delamination specimens for orthotropic materials. *J. Appl. Mech.* **57**, 627–634.

Soutis, C., Fleck, N. A. and Smith, P. A. (1991). Compression fatigue behavior of notched carbon fiber–epoxy laminates. *Int. J. Fatigue* **13**, 303–312.

Whitcomb, J. D. (1981). Experimental and analytical study of fatigue damage in notched graphite/epoxy laminates. *Fatigue of Fibrous Composites*, ASTM STP 723, pp. 48–53. Philadelphia, PA.

APPENDIX A

In this Appendix, we list the stress functions used in eqns (34) and (35) in text. With the use of the following expressions

$$\zeta_\alpha = \frac{z_\alpha - \sqrt{z_\alpha^2 - a^2 - s_\alpha^2 b^2}}{a + is_\alpha b} \quad \alpha = 1,2 \tag{A1}$$

$$\eta_{\alpha 1}^0 = \frac{z_\alpha^0 + \sqrt{(z_\alpha^0)^2 - a^2 - s_\alpha^2 b^2}}{a + is_\alpha b} \quad \alpha = 1,2 \tag{A2}$$

$$\eta_{\alpha 2}^0 = \frac{\bar{z}_\alpha^0 + \sqrt{(\bar{z}_\alpha^0)^2 - a^2 - \bar{s}_\alpha^2 b^2}}{a - i\bar{s}_\alpha b} \quad \alpha = 1,2 \tag{A3}$$

$$D\zeta_\alpha = -\frac{\zeta_\alpha}{\sqrt{z_\alpha^2 - a^2 - s_\alpha^2 b^2}} \quad \alpha = 1,2 \tag{A4}$$

where $z_\alpha = x + s_\alpha y$, $z_\alpha^0 = x_0 + s_\alpha y_0$, and $\bar{z}$ denotes the complex conjugate of a complex variable z, one can express these functions as follows

$$F_{1y}(z_1, z_{10}, z_{20}) = \lambda^{-1/4}\left[\frac{1}{(n+m)}\ln(\xi_1 - \eta_{11}^0) - \frac{n}{m}\frac{1}{(n+m)}\ln(\xi_1 - \eta_{12}^0) + \frac{1}{m}\ln(\xi_1 - \eta_{22}^0)\right] \tag{A5}$$

$$F_{1x}(z_1, z_{10}, z_{20}) = i\lambda^{-1/2}\left[-\ln(\zeta_1 - \eta_{11}^0) - \frac{n}{m}\ln(\zeta_1 - \eta_{12}^0) + \frac{n-m}{m}\ln(\zeta_1 - \eta_{22}^0)\right] \tag{A6}$$

$$F_{2y}(z_2, z_{10}, z_{20}) = \lambda^{-1/4}\left[-\frac{1}{n-m}\ln(\zeta_2 - \eta_{21}^0) - \frac{n}{m(n-m)}\ln(\zeta_2 - \eta_{22}^0) + \frac{1}{m}\ln(\zeta_2 - \eta_{12}^0)\right] \tag{A7}$$

$$F_{2x}(z_2, z_{10}, z_{20}) = i\lambda^{-1/2}\left[\ln(\zeta_2 - \eta_{21}^0) - \frac{n}{m}\ln(\zeta_2 - \eta_{22}^0) + \frac{n+m}{m}\ln(\zeta_2 - \eta_{12}^0)\right]. \tag{A8}$$

To list the kernel functions used in the integral equations (36) and (37) in text, we introduce following auxiliary functions:

$$f_{xx}^0(x, y, x_0, y_0) = 2\,\mathrm{Im}\left[\frac{(n+m)^2}{z_1 - z_{10}} - \frac{(n-m)^2}{z_2 - z_{20}}\right] \tag{A9}$$

$$f_{xy}^0(x, y, x_0, y_0) = 2\,\mathrm{Re}\left[\frac{(n+m)}{z_1 - z_{10}} - \frac{(n-m)}{z_2 - z_{20}}\right] \tag{A10}$$

$$f_{yx}^0(x, y, x_0, y_0) = 2\,\mathrm{Im}\left[\frac{i(n+m)}{z_1 - z_{10}} - \frac{i(n-m)}{z_2 - z_{20}}\right] \tag{A11}$$

$$f_{yy}^0(x, y, x_0, y_0) = 2\,\mathrm{Re}\left[\frac{i}{z_1 - z_{10}} - \frac{i}{z_2 - z_{20}}\right] \tag{A12}$$

$$g_{x1} = -\frac{1}{\zeta_1 - \eta_{11}^0} - \frac{n}{m}\frac{1}{\zeta_1 - \eta_{12}^0} + \frac{n-m}{m}\frac{1}{\zeta_1 - \eta_{22}^0} \tag{A13}$$

$$g_{x2} = \frac{1}{\zeta_2 - \eta_{21}^0} - \frac{n}{m}\frac{1}{\zeta_2 - \eta_{22}^0} + \frac{n+m}{m}\frac{1}{\zeta_2 - \eta_{12}^0} \tag{A14}$$

$$g_{y1} = \frac{1}{\zeta_1 - \eta_{11}^0} - \frac{n}{m}\frac{1}{\zeta_1 - \eta_{12}^0} + \frac{n+m}{m}\frac{1}{\zeta_1 - \eta_{22}^0} \tag{A15}$$

$$g_{y2} = \frac{1}{\zeta_2 - \eta_{21}^0} + \frac{n}{m}\frac{1}{\zeta_2 - \eta_{22}^0} - \frac{n-m}{m}\frac{1}{\zeta_2 - \eta_{12}^0} \tag{A16}$$

$$f_{xx}(x, y, x_0, y_0) = 2\,\mathrm{Im}\left[g_{x1}(n+m)^2 D\zeta_1 + g_{x2}(n-m)^2 D\zeta_2\right] \tag{A17}$$

$$f_{xy}(x, y, x_0, y_0) = 2\,\mathrm{Re}\left[-g_{y1}(n+m)D\zeta_1 + g_{y2}(n-m)D\zeta_2\right] \tag{A18}$$

$$f_{yx}(x, y, x_0, y_0) = 2\,\mathrm{Im}\left[i(n+m)g_{x1}D\zeta_1 + i(n-m)g_{x2}D\zeta_2\right] \tag{A19}$$

$$f_{yy}(x, y, x_0, y_0) = 2\,\mathrm{Re}\left[-ig_{y1}D\zeta_1 + ig_{y2}D\zeta_2\right]. \tag{A20}$$

Then the kernel functions are

$$\begin{aligned} k_{xx}(y, y_0) = {} & f_{xx}^0(a, y, -a, y_0) - f_{xx}^0(a, y, a, -y_0) - f_{xx}^0(a, y, -a, -y_0) + f_{xx}(a, y, a, y_0) \\ & - f_{xx}(a, y, a, -y_0) + f_{xx}(a, y, -a, y_0) - f_{xx}(a, y, -a, -y_0) \end{aligned} \tag{A21}$$

$$\begin{aligned} k_{xy}(y, y_0) = {} & f_{xy}^0(a, y, a, y_0) + f_{xy}^0(a, y, a, -y_0) - f_{xy}^0(a, y, -a, y_0) - f_{xy}^0(a, y, -a, -y_0) \\ & + f_{xy}(a, y, a, y_0) + f_{xy}(a, y, a, -y_0) - f_{xy}(a, y, -a, y_0) - f_{xy}(a, y, -a, -y_0) \end{aligned} \tag{A22}$$

$$k_{yx}(y,y_0)=f^0_{yx}(a,y,a,y_0)+f^0_{yx}(a,y,-a,y_0)-f^0_{yx}(a,y,a,-y_0)-f^0_{yx}(a,y,-a,-y_0)$$
$$+f_{yx}(a,y,a,y_0)-f_{yx}(a,y,a,-y_0)+f_{yx}(a,y,-a,y_0)-f_{yx}(a,y,-a,-y_0)$$
$$-\lambda^{-1/4}\mu k_{xx}(y,y_0)-\lambda^{-1/4}\mu f^0_{xx}(a,y,a,y_0) \quad \text{(A23)}$$

$$k_{yy}(y,y_0)=f^0_{yy}(a,y,a,-y_0)-f^0_{yy}(a,y,-a,y_0)-f^0_{yy}(a,y,-a,-y_0)+f_{yy}(a,y,a,y_0)$$
$$+f_{yy}(a,y,a,-y_0)-f_{yy}(a,y,-a,y_0)-f_{yy}(a,y,-a,-y_0)-\lambda^{-1/4}\mu k_{yx}(y,y_0). \quad \text{(A24)}$$